Accurate Statistical Model of Radiation Patterns in Analog Beamforming Including Random Error, Quantization Error, and Mutual Coupling

Seunghoon Lee, *Member, IEEE*, and Ho-Jin Song, *Senior Member, IEEE*

***Abstract*— Analog beamforming technology is being used to overcome various technical drawbacks of mm-wave wireless communications systems. However, the errors caused by circuit implementations, quantized control, and imperfect isolation between antenna elements result in radiation pattern (RP) distortion and performance deterioration. In particular, the quantization error and mutual coupling cause the active reflection coefficient (ARC) of each antenna element to vary with respect to the main beam direction, resulting in statistical behavior changes depending on steering angles. In this article, we derive the statistical behavior of RPs with all those dominant errors taken into account. The analysis reveals that Beckmann distribution offers the exact solution for the cumulative distribution of the sidelobe level (SLL), which is very consistent with a Monte Carlo simulation including the ARC. In addition, the Rician distribution reflecting the three errors exhibits overall good accuracy, with inherent deviation from the Monte Carlo simulation results at certain steering angles due to the approximation of uncorrelated RPs and identical variances that are not valid in real antenna arrays. Our analysis also indicates that, to define the maximum probability of exceeding a certain SLL, the variance and correlation should be considered along with the mean of the RPs.**

***Index Terms*— Antenna radiation patterns (RPs), error analysis, mutual coupling, random noise.**

I. Introduction

WIRELESS data traffic is exponentially increasing day by day. To accommodate this trend and meet the demand for larger data capacity, fifth-generation (5G) mobile communications at mm-wave frequencies have been developed, where rich spectral resources are available [1]. The analog beamforming scheme made the 5G system a reality by overcoming the drawbacks arising from mm-waveband operation, such as limited signal to noise ratios and high atmospheric attenuation loss. However, in analog beamforming, radiation pattern (RP) distortion cannot be avoided because of implementation errors, quantized control, and imperfect isolation between antenna elements. The sidelobe level (SLL) rises and, therefore, interference due to radiation transmitted to or received from undesired directions degrades total system performance. If the implementation errors could be precisely measured and characterized, we would be able to completely compensate for the RP distortion [2]–[4]. Unfortunately, considering the mass production of silicon-based analog beamforming transceivers for 5G and car radar systems [5], it is often impractical to measure and calibrate all manufactured transceivers. Therefore, a precise statistical analysis tool is necessary. The purpose of this article is to estimate the effects of random error, quantization error, and mutual coupling on the system performance, especially the RP. Once we have accurate knowledge about the major origins of RP distortion, many costly and time-consuming calibration processes can be omitted.

Random and quantization errors have mainly been considered in analyzing the statistical behavior of the RP and SLL. Ruze [6] proved that the RP follows the Rician distribution function under the random error condition. The study was extended to estimate the probability function of the peak SLL and analyze system performance [7]. In addition, to analyze the adverse effects of a digitally controlled phase shifter, phase quantization error was modeled as a uniform random process and the RP distribution was approximated with the Rician function as well [8]. However, since the variances of the real and imaginary parts of the RP were assumed to be equal and independent for the Rician distribution, these studies would underestimate RP distortion. In [9], it was shown that the Beckmann distribution provides a more accurate analysis, but only the random error was considered.

The two other dominant factors causing RP distortion and determining the statistical behavior of the SLL are quantization error and mutual coupling [10]. The quantization error that arises from the discrete nature of digitally controlled attenuators and phase shifters is strongly coupled to the steering angle and beam shaping algorithm. It should, therefore, be modeled as a deterministic variable in a specific beam direction instead of as a uniform random process [11], [12]. Mutual coupling is an interchannel effect by which signals fed to each antenna couple with each other. The input impedance of each antenna element, namely the active reflection coefficient (ARC), can change when the excitation of adjacent element varies. The ARC varies depending on the excitation amplitudes and phases

Manuscript received May 6, 2020; revised October 27, 2020; accepted November 25, 2020. Date of publication January 8, 2021; date of current version July 7, 2021. This work was supported by the Institute of Information & communications Technology Planning & Evaluation (IITP) funded by the Korea Government (MSIT) under Grant IITP-2018-0-00823, Investigation on future mm-Wave circuits, packages, and system and the BK21 plus program through the National Research Foundation (NRF) funded by MSIT. *(Corresponding author: Ho-Jin Song.)*

The authors are with the Department of Electrical Engineering, Pohang University of Science and Technology, Pohang 37673, South Korea (e-mail: seunghoon.lee@postech.ac.kr; hojin.song@postech.ac.kr).

Color versions of one or more figures in this article are available at https://doi.org/10.1109/TAP.2020.3048528.

Digital Object Identifier 10.1109/TAP.2020.3048528

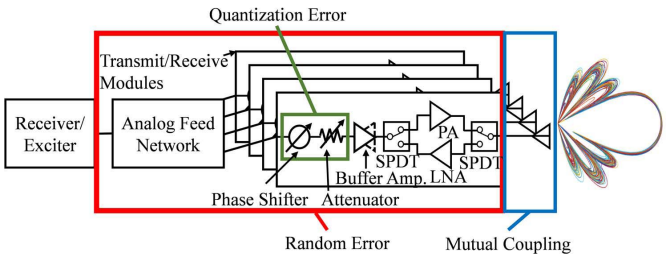

Fig. 1. Analog phased array architecture and the causes of RP distortion.

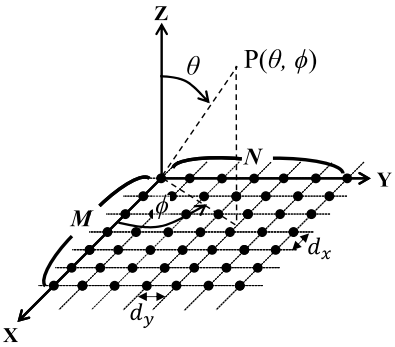

Fig. 2. $M \times Np$ lanar array on rectangular grid with element spacing d_x in the x-direction and d_y in the y-direction.

for antenna elements [13], [14], causing further distortion of the RPs [3], [15].

In this article, we derive two statistical behavior functions of RPs using random Gaussian errors, the quantization step in amplitude and phase, and the mutual coupling represented by S-parameters. The exact solution based on the Beckmann distribution function offers very good agreement with Monte Carlo simulation results regardless of the steering directions and observation angles, such as the azimuth and elevation. Assuming the real and imaginary components of RPs are uncorrelated and possess identical variance, the exact solution can be approximated in the Rician function. However, unlike in prior work, the approximate solution represents the effect of the quantized phase control and the mutual coupling between antenna elements and provides the probability distribution of the SLL as a function of the steering angle with reasonable overall accuracy. In addition, the developed solutions reveal that the maximum probability of the SLL's exceeding a certain level will not always be given at the peak sidelobe of the RPs' mean. For the interference analysis, the variance of the RPs must be taken into account as well.

This article is organized as follows. Section II shows how we model the random errors, quantization errors, and mutual coupling. In Section III, the distorted RP due to these three factors is mathematically modeled, followed by the statistical derivation of parameters such as the mean and variance in Section IV. In Section V, we derive the exact and approximate probability distribution function (PDF) and cumulative distribution function (CDF) solutions based on Beckmann and Rician distributions and compare the solutions with Monte Carlo simulation results for verification. Finally, we conclude this article in Section VI.

II. Cause of RP Distortion

As illustrated in Fig. 1, an analog phased array antenna for 5G consists of digitally controlled phase shifters and attenuators, amplifiers, antennas, and feed networks. The array system suffers from three major errors: random error, quantization error, and mutual coupling [6], [7], [14], [16].

Consider a rectangular planar array with the elements arranged on the xy plane, as shown in Fig. 2. In the ideal case, the relationship between antenna aperture voltages V_{mn} and complex weights A_{mn} for the mnth element of $M \times N$ planar array can be modeled as

$$V_{mn} = \alpha V_{\text{ant}} A_{mn} \tag{1}$$

where V_{ant} is the common transmitted or received signal of the analog beamforming system and antenna element index, $m = 1, \ldots, M$, $n = 1, \ldots, N$. α is a complex constant representing the transfer function of the errorless RF chains, excluding the phase shifter and attenuator. For beam steering in the direction (θ_0, ϕ_0), in the case with no error, one sets the phase shifter to satisfy $\angle A_{m+1,n+1} - \angle A_{mn} = -kd_x \sin\theta_0 \cos\phi_0 - kd_y \sin\theta_0 \sin\phi_0$, where k, d_x, and d_y are the wavenumber, the distance between adjacent antenna elements arrayed in the x-direction, and the distance between adjacent antenna elements arrayed in the y-direction, respectively. The amplitude of A_{mn} is determined depending on the amplitude tapering. In this article, Dolph–Chebyshev window that is one of the popular amplitude tapering is used for sidelobe suppression. In addition, A_{mn} is normalized to make the maximum level of the RP unity, as was done in previous work [6], [7], [9]. For simplicity, we assume V_{ant} and α are equal to 1. The relative amplitude error e^{A}_{mn} and phase error e^{P}_{mn} can be added to (1) as follows [6], [7]:

$$V_{mn} = e_r A_{mn} = \left(1 + e^{\text{A}}_{mn}\right) e^{j e^{\text{P}}_{mn}} \cdot A_{mn}. \tag{2}$$

A. Random Error

The performance of different channels of mass-produced radio frequency (RF) transceivers is not identical because of implementation errors associated with, for instance, the manufacturing tolerance of semiconductor devices, packaging, and antenna feeding networks. The doping concentration, thickness of silicon dioxide, graininess of polysilicon, and electrical characteristics of package wiring structures are not constant throughout the manufacturing process [17]. The gain and phase errors of each RF channel usually exhibit a Gaussian distribution characterized by its mean and standard deviation [18], [19]. For example, a recent CMOS phased-array mm-wave transceiver showed 0.8 dB and 6° standard deviation of gain and phase errors between channels, respectively [20]. Then, antenna aperture voltages distorted by the random error for the mnth element, V^R_{mn}, can be modeled as

$$V^R_{mn} = A_{mn} e^R_{mn} = A_{mn}\left(1 + \delta^{\text{A}}_{mn}\right) e^{j\delta^{\text{P}}_{mn}} \tag{3}$$

where A_{mn} is a normalized ideal complex weight, and δ^{A}_{mn} and δ^{P}_{mn} are amplitude and phase random variables, respectively,

which have a zero mean Gaussian distribution for the *mn*th antenna element.

B. Quantization Error

The quantization error arises from the discrete nature of digitally controlled units, such as variable gain amplifiers or attenuators and phase shifters. The roundoff error occurs when a continuous random variable is converted to a discrete variable. If the quantized control step is not fine enough, the RP may be distorted [21].

If the least significant bit (LSB) of an attenuator and phase shifter is

$$\mathrm{LSB^A(dB)} = \beta \tag{4}$$

$$\mathrm{LSB^P(radians)} = \frac{2\pi}{2^{Np}} \tag{5}$$

where β is a constant and N_p is the number of phase control bits, and the quantized complex excitation weight A_{mn}^{Q} will be

$$20\times\log_{10}\left(\left|A_{mn}^{Q}\right|\right) = \mathrm{LSB^A}\times\mathrm{round}\left(\frac{20\times\log_{10}(|A_{mn}|)}{\mathrm{LSB^A}}\right) \tag{6}$$

$$\angle A_{mn}^{Q}(\mathrm{radians}) = \mathrm{LSB^P}\times\mathrm{round}\left(\frac{\angle A_{mn}}{\mathrm{LSB^P}}\right) \tag{7}$$

where round (B) returns a rounded decimal number, $|B|$ is the absolute value of complex value B, and $\angle B$ is the phase of complex value B. Then, the antenna aperture voltages distorted by the quantization error for the *mn*th element, V_{mn}^{Q}, can be similarly modeled as

$$V_{mn}^{Q} = A_{mn}e_{mn}^{Q} = A_{mn}\left(1+\Delta_{mn}^{\mathrm{A}}\right)e^{j\Delta_{mn}^{\mathrm{P}}} \tag{8}$$

where Δ_{mn}^{A} and Δ_{mn}^{P} are the amplitude and phase quantized errors, given below by using (6) and (7)

$$\Delta_{mn}^{\mathrm{A}} = \frac{\left|A_{mn}^{Q}\right|}{|A_{mn}|} - 1 \tag{9}$$

$$\Delta_{mn}^{\mathrm{P}} = \angle A_{mn}^{Q} - \angle A_{mn}. \tag{10}$$

C. Mutual Coupling and Mismatch

Random and quantization errors occur in each channel independently. In contrast, mutual coupling is an interchannel effect caused by the imperfect isolation between antenna elements. In general, mutual coupling is modeled as an N-by-N scattering matrix for an N-element linear array [3]. Similarly, $S_{mn,pq}$ can be used to represent the coupling between the *mn*th element and *pq*th element of an $M \times N$ planar array, $m = 1,\ldots,M$, $n = 1,\ldots,N$, $p = 1,\ldots,M$, and $q = 1,\ldots,N$. $S_{mn,pq}$ $(m = p$ and $n = q)$ is the reflection coefficient of the *mn*th element. $S_{mn,pq}$ $(m \neq p$ or $n \neq q)$ is the mutual coupling between an *mn*th element and *pq*th element. The magnitude and phase of elements $S_{mn,pq}(m \neq p$ or $n \neq q)$ strongly depend on the physical properties of array antennas, such as the dielectric substrate thickness, the type of antenna element, antenna cover or radome, and the distance between adjacent antennas [22]. Then, antenna aperture voltages distorted by the mutual coupling and impedance mismatching for the *mn*th element, V_{mn}^{MC}, will be given as

$$V_{mn}^{MC} = \sum_{p=1}^{M}\sum_{q=1}^{N} A_{pq}C_{mn,pq} \tag{11}$$

where $C_{mn,pq}$ represents the coupling between the *mn* element and *pq* element, which is defined as $C_{mn,pq} = I(mn, pq) + S_{mn,pq}$, where $I(mn, pq) = 1$ for $m = p$ and $n = q$; otherwise $I(mn, pq) = 0$. Equation (11) is an extended equation for mutual coupling and a planar array from a linear array [23], [24]. As can be seen in (11), the complex weights applied to the antennas are mixed by mutual coupling. Therefore, even if identical weights are applied to all antennas for broadside radiation, mutual coupling will distort the antenna aperture voltage at the edge antenna elements, and the RP will be distorted a little. In beam steering in a certain direction, the amplitude and phase errors due to mutual coupling will be different at each antenna element and vary as the steering angle changes. It is worth noting that we assumed that element aperture currents do not change in shape and thus the normalized element pattern does not change for each antenna element, which is a reasonable approximation for large antenna arrays or moderate-size ones but with dummy patterns.

D. Distorted Aperture Voltage

The aperture voltage distorted by the random error, quantization error, and mutual coupling, V_{mn}^{D}, can be expressed as follows using (3), (8), and (11):

$$\begin{aligned} V_{mn}^{D} &= \sum_{p=1}^{M}\sum_{q=1}^{N} A_{pq}e_{pq}^{R}e_{pq}^{Q}C_{mn,pq} \\ &= \sum_{p=1}^{M}\sum_{q=1}^{N} A_{pq}C_{mn,pq}\left(1+\delta_{pq}^{\mathrm{A}}\right)\left(1+\Delta_{pq}^{\mathrm{A}}\right)e^{j\left(\delta_{pq}^{\mathrm{P}}+\Delta_{pq}^{\mathrm{P}}\right)}. \end{aligned} \tag{12}$$

III. Mathematical Model of Array Pattern

The errors and mutual coupling mentioned above result in RP distortion. In this section, the array RP under the errors and mutual coupling is expressed mathematically.

In general, the ideal RP of a phased-array antenna, $F(\theta, \phi)$, is given as the product of a single element radiation factor $f(\theta, \phi)$ and the array pattern of isotropic point sources located on the xy plane of a planar array [25]

$$F(\theta,\phi) = f(\theta,\phi)\cdot\sum_{m=1}^{M}\sum_{n=1}^{N} V_{mn}e^{j(mu+nv)} \tag{13}$$

$$u = kd_x\cos\phi\sin\theta, v = kd_y\sin\phi\sin\theta \tag{14}$$

where θ and ϕ are the elevation and azimuth angle. V_{mn} is the antenna aperture voltage that is applied to the *mn*th element. If we assume that a planar array is composed of homogeneous and isotropic $(f(\theta, \phi) = 1)$ elements, the RP of an *MN*-element planar array can be simplified as

$$F(\theta,\phi) = \sum_{m=1}^{M}\sum_{n=1}^{N} V_{mn}e^{j(mu+nv)}. \tag{15}$$

From (13) and (15), we can find the distorted RP $F_d(\theta)$ under the random and quantization errors and mutual coupling. Here, we assume that the random and quantization errors at each channel are independent and uncorrelated to each other

$$\begin{aligned} &F_d(\theta,\phi) \\ &= \sum_{m=1}^{M}\sum_{n=1}^{N} V_{mn}^{D} e^{j(mu+nv)} \\ &= \sum_{m=1}^{M}\sum_{n=1}^{N}\left(\sum_{p=1}^{M}\sum_{q=1}^{N} A_{pq}C_{mn,pq}\left(1+\delta_{pq}^{\mathrm{A}}\right)\left(1+\Delta_{pq}^{\mathrm{A}}\right)e^{j\left(\delta_{pq}^{\mathrm{P}}+\Delta_{pq}^{\mathrm{P}}\right)}\right) \\ &\quad \times e^{j(mu+nv)}. \end{aligned} \tag{16}$$

We assume both random variables follow the Gaussian distribution with zero-means, shown as follows:

$$\delta_{mn}^{\mathrm{A}} \sim \mathcal{N}\left(0,\sigma_a^2\right) \tag{17}$$

$$\delta_{mn}^{\mathrm{P}} \sim \mathcal{N}\left(0,\sigma_p^2\right) \tag{18}$$

where σ_a^2 and σ_p^2 are the variances of the amplitude and phase random errors.

Fig. 3 illustrates a hundred examples of possible distorted RPs from an 8×8 planar array directed to ($\theta_0 = 30°$, $\phi_0 = 0°$) with a -25 dB Dolph–Chebyshev window and half-lambda antenna spacing, along with the ideal RP with no errors. As can be seen, the RP fluctuates a lot due to the errors, which should be investigated by statistical analysis.

IV. Statistical Quantities

The distorted RP in (16) can be divided into real and imaginary values, given as follows:

$$\begin{aligned} &R_{RP}(\theta,\phi) \\ &\quad = R_{RP} = \mathrm{Re}(F_d(\theta,\ \phi)) \\ &\quad = \sum_{m=1}^{M}\sum_{n=1}^{N}\sum_{p=1}^{M}\sum_{q=1}^{N}\mathrm{Re}\left(A_{pq}C_{mn,pq}\left(1+\delta_{pq}^{\mathrm{A}}\right)\left(1+\Delta_{pq}^{\mathrm{A}}\right)\right. \\ &\qquad\qquad \left.\times e^{j\left(\delta_{pq}^{\mathrm{P}}+\Delta_{pq}^{\mathrm{P}}\right)}e^{j(mu+nv)}\right) \end{aligned} \tag{19}$$

$$\begin{aligned} &I_{RP}(\theta,\phi) \\ &\quad = I_{RP} = \mathrm{Im}(F_d(\theta,\phi)) \\ &\quad = \sum_{m=1}^{M}\sum_{n=1}^{N}\sum_{p=1}^{M}\sum_{q=1}^{N}\mathrm{Im}\left(A_{pq}C_{mn,pq}v\left(1+\delta_{pq}^{\mathrm{A}}\right)\left(1+\Delta_{pq}^{\mathrm{A}}\right)\right. \\ &\qquad\qquad \left.\times e^{j\left(\delta_{pq}^{\mathrm{P}}+\Delta_{pq}^{\mathrm{P}}\right)}e^{j(mu+nv)}\right) \end{aligned} \tag{20}$$

where Re (B) and Im (B) are real and imaginary values of B.

Here, we first derive the expected values of R_{RP} and I_{RP}, their variances, and the covariance between them and then examine how well the Rician and Beckmann distributions describe the statistical behavior of the RP under the three major error conditions by comparing the results with Monte Carlo simulations.

A. Expected Value

Once we assume a certain beam direction, the effects from the quantization error and mutual coupling can be considered as deterministic variables instead of random ones. Thus, from (19) and (20), the expected values of R_{RP} and I_{RP}, μ_R and μ_I, respectively, can be written as

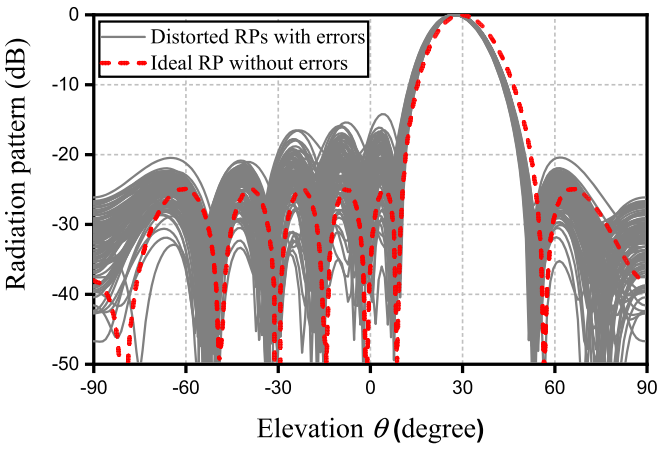

Fig. 3. Distorted RPs $F_d(\theta, 0)$ of an 8×8 planar array with a -25 dB Dolph–Chebyshev window due to random error, quantization error, mutual coupling, and ideal pattern $F(\theta, 0)$. For the calculation, we assumed all errors with the parameters $\sigma_a = 1.0$ dB, $\sigma_p = 10.0°$, $\mathrm{LSB}^{\mathrm{A}} = 1.0$ dB, $\mathrm{LSB}^{\mathrm{P}} = 11.25°$, $|S_{mm,pq}| = -12$ dB, and $\angle S_{mn,pq} = 20°$ for $|m-p|+|n-q| = 1$; $|S_{mn,pq}| = -24$ dB and $\angle S_{mn,pq} = -20°$ for $|m-p|+|n-q| = 2$, $|m-p| \neq 1$, and $|n-q| \neq 1$; $|S_{mn,pq}| = -20$ dB and $\angle S_{mn,pq} = -30°$ for $|m-p| = 1$ and $|n-q| = 1$.

$$\begin{aligned} \mathrm{E}[R_{RP}] &= \mu_R \\ &= \sum_{m=1}^{M}\sum_{n=1}^{N}\sum_{p=1}^{M}\sum_{q=1}^{N}\mathrm{Re}\left(A_{pq}C_{mn,pq}\mathrm{E}\left[\left(1+\delta_{pq}^{\mathrm{A}}\right)\right]\mathrm{E}\left[e^{j\delta_{pq}^{\mathrm{P}}}\right]\right. \\ &\qquad \left.\cdot\left(1+\Delta_{pq}^{\mathrm{A}}\right)e^{j\Delta_{pq}^{\mathrm{P}}}e^{j(mu+nv)}\right) \end{aligned} \tag{21}$$

$$\begin{aligned} \mathrm{E}[I_{RP}] &= \mu_I \\ &= \sum_{m=1}^{M}\sum_{n=1}^{N}\sum_{p=1}^{M}\sum_{q=1}^{N}\mathrm{Im}\left(A_{pq}C_{mn,pq}\mathrm{E}\left[\left(1+\delta_{pq}^{\mathrm{A}}\right)\right]\mathrm{E}\left[e^{j\delta_{pq}^{\mathrm{P}}}\right]\right. \\ &\qquad \left.\cdot\left(1+\Delta_{pq}^{\mathrm{A}}\right)e^{j\Delta_{pq}^{\mathrm{P}}}e^{j(mu+nv)}\right) \end{aligned} \tag{22}$$

where $\mathrm{E}[B]$ is the mean of the random variable B. According to (17), (18), and the Maclaurin series of the exponential function (A-18), the expected values of $(1+\delta_{mn}^{\mathrm{A}})$ and $e^{j\delta_{mn}^{\mathrm{P}}}$ are given as

$$\mathrm{E}\left[1+\delta_{mn}^{\mathrm{A}}\right] = 1 \tag{23}$$

$$\begin{aligned} \mathrm{E}\left[e^{j\delta_{mn}^{\mathrm{P}}}\right] &= \int_{-\infty}^{\infty} e^{j\delta_{mn}^{\mathrm{P}}} d\delta_{mn}^{\mathrm{P}} \\ &= \int_{-\infty}^{\infty}\left(1+j\delta_{mn}^{\mathrm{P}} - \frac{\left(\delta_{mn}^{\mathrm{P}}\right)^2}{2} - j\frac{\left(\delta_{mn}^{\mathrm{P}}\right)^3}{6}+\ldots\right) \\ &\quad \times d\delta_{mn}^{\mathrm{P}} = e^{-\sigma_p^2/2}. \end{aligned} \tag{24}$$

If we substitute (23) and (24) into (21) and (22), μ_R and μ_I can be written as

$$\begin{aligned} \mu_R = e^{-\sigma_p^2/2}\cdot &\sum_{m=1}^{M}\sum_{n=1}^{N}\sum_{p=1}^{M}\sum_{q=1}^{N}\mathrm{Re}\left(\left|A_{pq}C_{mn,pq}\left(1+\Delta_{pq}^{\mathrm{A}}\right)\right|\right. \\ &\left.\cdot e^{j\left(\angle A_{pq}+\angle C_{mn,pq}+\Delta_{pq}^{\mathrm{P}}\right)}e^{j(mu+nv)}\right) \end{aligned} \tag{25}$$

$$\mu_I = e^{-\sigma_p^2/2} \cdot \sum_{m=1}^{M}\sum_{n=1}^{N}\sum_{p=1}^{M}\sum_{q=1}^{N} \mathrm{Im}\Big(\big|A_{pq}C_{mn,pq}\big(1+\Delta_{pq}^{\mathrm{A}}\big)\big| \cdot e^{j\left(\angle A_{pq}+\angle C_{mn,pq}+\Delta_{pq}^{\mathrm{P}}\right)} e^{j(mu+nv)}\Big). \tag{26}$$

The magnitude of the RP's mean, h, can be expressed as

$$h = \sqrt{\mu_R^2 + \mu_I^2}. \tag{27}$$

B. Variance

We omit the detailed derivation of the variance for R_{RP} and I_{RP}, which can be found in the appendix. The variances of R_{RP} and I_{RP}, σ_R^2 and σ_I^2, respectively, are derived as

$$\mathrm{Var}[R_{RP}] = \sigma_R^2 = \mathrm{A} + \mathrm{B} \tag{28}$$

$$\mathrm{Var}[I_{RP}] = \sigma_I^2 = \mathrm{A} - \mathrm{B} \tag{29}$$

where

$$\mathrm{A} = \frac{1}{2}\Big(1+\sigma_a^2 - e^{-\sigma_p^2}\Big) \cdot \sum_{m=1}^{M}\sum_{n=1}^{N}\sum_{a=1}^{M}\sum_{b=1}^{N}\sum_{p=1}^{M}\sum_{q=1}^{N}\Big(\Big|C_{mn,pq}C_{ab,pq}A_{pq}^2\big(1+\Delta_{pq}^{\mathrm{A}}\big)^2\Big| \cdot e^{j\left(\angle C_{mn,pq}-\angle C_{ab,pq}\right)} e^{j[(m-a)u+(n-b)v]}\Big) \tag{30}$$

$$\mathrm{B} = \frac{1}{2}\Big(\big(1+\sigma_a^2\big)e^{-2\sigma_p^2} - e^{-\sigma_p^2}\Big) \cdot \sum_{m=1}^{M}\sum_{n=1}^{N}\sum_{a=1}^{M}\sum_{b=1}^{N}\sum_{p=1}^{M}\sum_{q=1}^{N}\mathrm{Re}\Big(\big|C_{mn,pq}C_{ab,pq}A_{pq}^2\big(1+\Delta_{pq}^{\mathrm{A}}\big)^2\big| \cdot e^{j\left(\angle C_{mn,pq}+\angle C_{ab,pq}+2\cdot\angle A_{pq}+2\cdot\Delta_{pq}^{\mathrm{P}}\right)} e^{j[(m+a)u+(n+b)v]}\Big). \tag{31}$$

As shown in (30) and (31), because of the mutual coupling terms $\mathrm{C}_{mn,pq}$ ($m \neq p$ or $n \neq q$), A and B depend on u and v, which, as defined in (14), is a function of θ and ϕ. Therefore, the variances of R_{RP} and I_{RP} are also a function of θ and ϕ. In addition, from (28) and (29), the two variances are not identical as long as B is not zero, and the difference (i.e., $2 \cdot \mathrm{B}$) is a function of θ and ϕ as well.

Following an approach similar to that in [6], we can define the average variance σ_{aver}^2 as

$$\sigma_{aver}^2 = \frac{\mathrm{Var}[R_{RP}] + \mathrm{Var}[I_{RP}]}{2} = \mathrm{A}. \tag{32}$$

Again, σ_{aver}^2 is not independent of θ and ϕ, whereas prior work assumed that it is. If the mutual coupling is ignorable, that is if $\mathrm{C}_{mn,pq} = 1$ ($m = p$ and $n = q$) and $\mathrm{C}_{mn,pq} = 0$ ($m \neq p$ or $n \neq q$), summation terms in (30) go to zero unless $m = p = a$ and $n = q = b$, resulting in constant σ_{aver}^2 with respect to θ and ϕ, as prior work assumed. Meanwhile, it is worth noting that the difference between the two variances will not be independent of θ and ϕ even if there is no mutual coupling. If the mutual coupling is not ignorable, σ_{aver}^2 changes according to θ and ϕ. Then, the average variance at certain θ and ϕ can be higher than the average variance with no mutual coupling. If designers are interested in the maximum probability of exceeding a certain SLL, the probability of SLL calculating at an angle where h is highest as previous works did [6], [7], [9] will not always the maximum probability. In Section VI-B, a statistical analysis of this behavior is presented.

C. Correlation Coefficient

Correlation coefficient ρ_{RI} is mathematically defined as

$$\rho_{RI} = \frac{\mathrm{Cov}(R_{RP}, I_{RP})}{\sqrt{\mathrm{Var}[R_{RP}]} \cdot \sqrt{\mathrm{Var}[I_{RP}]}}. \tag{33}$$

The covariance between R_{RP} and $I_{RP}\mathrm{Cov}(R_{RP}, I_{RP})$ can be derived as (see appendix for details)

$$\begin{aligned}&\mathrm{Cov}(R_{RP}, I_{RP})\\ &= \mathrm{E}[(R_{RP} - \mathrm{E}[R_{RP}])(I_{RP} - \mathrm{E}[I_{RP}])]\\ &= \frac{1}{2}\left(\left(1+\frac{2}{\sigma_a}\right)e^{-2\sigma_p^2} - e^{-\sigma_p^2}\right)\\ &\quad\cdot \sum_{m=1}^{M}\sum_{n=1}^{N}\sum_{a=1}^{M}\sum_{b=1}^{N}\sum_{p=1}^{M}\sum_{q=1}^{N}\mathrm{Im}\Big(\Big|C_{mn,pq}C_{ab,pq}A_{pq}^2\big(1+\Delta_{pq}^{\mathrm{A}}\big)^2\Big|\\ &\quad\cdot e^{j\left(\angle C_{mn,pq}+\angle C_{ab,pq}+2\cdot\angle A_{pq}+2\cdot\Delta_{pq}^{\mathrm{P}}\right)} e^{j[(m+a)u+(n+b)v]}\Big).\end{aligned} \tag{34}$$

Unlike in prior work [6], [7], it is clearly shown that R_{RP} and I_{RP} are correlated and the covariance is also θ and ϕ dependent.

The θ and ϕ dependence of the statistical properties derived above eventually affects the statistical behavior. The details will be discussed in Section V and VI with examples.

V. Verification of Statistical Analysis

Based on the statistical quantities of R_{RP} and I_{RP} in Section IV, we derive the exact and approximate PDF and CDF solutions that are based on Beckmann and Rician distributions. Using Monte Carlo simulation, we will verify the solutions for random and quantization errors and mutual coupling effects. In addition, we will examine how those errors affect the statistical behavior of the SLL, such as the maximum probability of the SLL's exceeding a certain level x_0, $p_{\max}(x)$, which is given as

$$p_{\max}(x_0) = \int_{x_0}^{\infty} \mathrm{PDF}(x)dx = 1 - \mathrm{CDF}(x_0) \tag{35}$$

where x and x_0 are the magnitude of the RP and reference level for the maximum probability. PDF and CDF are the probability density function and cumulative distributed function of the RP magnitude, x.

A. Beckmann and Rician Distribution

Real and imaginary components of the antenna RP are commonly assumed to follow the Gaussian distribution by the central limit theorem. Therefore, the magnitude of the RP can be modeled with Beckmann and Rician distribution functions [6], [9].

Since the real and imaginary components of the distorted RP are correlated as shown in (33) and (34), the Beckmann function provides an exact solution for the statistical behavior of

the distorted RP, which is defined as [26]

$$PDF_{Beck}(x) = \frac{x}{2\pi\sigma_R\sigma_I\sqrt{1-\rho_{RI}^2}}\int_0^{2\pi} e^{-z/(1-\rho_{RI}^2)}d\theta \quad (36)$$

with

$$z = \frac{(x\cos\theta-\mu_R)^2}{2\sigma_R^2} + \frac{(x\sin\theta-\mu_I)^2}{2\sigma_I^2} - \frac{\rho_{RI}(x\cos\theta-\mu_R)(x\sin\theta-\mu_I)}{\sigma_R\sigma_I} \quad (37)$$

where x is the magnitude of the sum of two Gaussian distributions. The CDF of the Beckmann PDF can be calculated by

$$CDF_{Beck}(x) = \int_0^x PDF_{Beck}(x')dx'. \quad (38)$$

On the other hand, if we ignore the difference between the two variances and assume the two Gaussian distributions are uncorrelated, the magnitude of the distorted RP can be approximated by the Rician PDF as

$$PDF_{Rician}(x) = \frac{x}{\sigma_{aver}^2}e^{-(x^2+h^2)/(2\sigma_{aver}^2)}I_0\left(\frac{xh}{\sigma_{aver}^2}\right) \quad (39)$$

where I_0 is the modified Bessel function of the first kind with order zero. Using σ_{aver}^2 in (32) and (40) will provide an approximate solution under the three major errors. The CDF of the Rician PDF is defined as

$$CDF_{Rician}(x) = \int_0^x PDF_{Rician}(x')dx'. \quad (40)$$

It is worth noting that the Rician distribution has been used in previous works [6], [7], but they considered only random error. In contrast, the approximate solution in this work includes all three major origins of distortion with σ_{aver}^2.

B. Verification With Monte Carlo Simulation

To verify the derivations, we compared the calculated CDFs with the Beckmann and Rician distributions with the results of Monte Carlo simulation, which was conducted with (16). The values of the error parameters are listed in Table I. To extract the realistic mutual coupling parameters at 28.5 GHz, an 8×8 uniform rectangular array with patch antenna spacing of half-lambda was designed on a Rogers RT/duroid 5880 substrate with 0.787 mm thickness. Width and length were 4.23 and 3.2 mm, respectively. A coaxial-fed microstrip patch antenna was used because coupling occurs only between antenna elements in this structure. The coupling parameters were extracted from S-parameters calculated by using Ansoft HFSS software. For simplicity, we ignored mutual coupling parameters other than the first- and second-order neighboring ones. We assumed $S_{mn,pq}$ has the same value for $|m-p|+|n-q| = 1$, $S_{mn,pq}$ has the same value for $|m-p|+|n-q| = 2$ and $|m-p| \neq 1$, and $S_{mn,pq}$ has the same value for $|m-p| = 1$ and $|n-q| = 1$. To maintain the accuracy of the Monte Carlo simulation, 10 000 RPs were calculated under random and quantization errors and mutual coupling for several steering angles in the range from 0° to 60°.

TABLE I
PARAMETERS FOR ANALYSIS

Quantity	Values
Random error	$\sigma_a = 0.1$ dB, $\sigma_p = 10°$
Quantization error	$LSB^A = 0.5$ dB, $LSB^P = 5.625°$
Mutual coupling (planar array)	$\lvert S_{mn,pq}\rvert = -18$ dB, $\angle S_{mn,pq} = 30°$ for $\lvert m-p\rvert+\lvert n-q\rvert = 1$ $\lvert S_{mn,pq}\rvert = -22.8$ dB, $\angle S_{mn,pq} = -179°$ for $\lvert m-p\rvert+\lvert n-q\rvert = 2$ and $\lvert m-p\rvert \neq 1$ $\lvert S_{mn,pq}\rvert = -35$ dB, $\angle S_{mn,pq} = -112°$ for $\lvert m-p\rvert = 1 \& \lvert n-q\rvert = 1$
Mutual coupling (linear array)	$\lvert S_{1n,1q}\rvert = -14.5$ dB, $\angle S_{1n,1q} = -150°$ for $\lvert n-q\rvert = 1$ $\lvert S_{1n,1q}\rvert = -21.5$ dB, $\angle S_{1n,1q} = 10°$ for $\lvert n-q\rvert = 2$

Fig. 4 compares the SLL CDFs of an 8×8 planar antenna array at the angle of the peak sidelobe from the mean of RP magnitude h defined in (27). As can be seen in Fig. 4(a), the Beckmann CDFs agree very well with the Monte Carlo simulations for all three steering angles. This is obviously because the Beckmann function is the exact solution reflecting all major errors with no approximation. In contrast, as shown in Fig. 4(b), the CDF (black line) from prior work that considered only random error showed a significant difference from the Monte Carlo results and never changed with the beam steering. This can be understood from the mean and variance in (25), (26), and (32), which become independent of the steering angle when quantization error and mutual coupling are ignored. For small and low-cost phased array antennas with large mutual coupling and coarse digital control bits, the solution in [6] considering only the random implementation error is not good enough for accurate analysis. Ultimately, the Beckmann PDF considering all the errors and mutual coupling in this work will serve as an important basis of techniques for accurate phased array antenna calibration.

For the other Rician distribution in this work from (40), the approximated solution exhibits reasonable accuracy overall, with little deviation from the Monte Carlo simulation results at certain steering angles, as shown in Fig. 4(b). When steering angles θ_0 and ϕ_0 are both 30°, the maximum difference in the SLL between the two at the same cumulative probability is approximately 2.9 dB. Since we assumed that the real and imaginary components of the RP are independent, and that variances are identical to those averaged for the Rician function, such discrepancy cannot be avoided when the antenna exhibits unignorable correlation between the real and imaginary RPs. However, when the steering angles θ_0 and ϕ_0 are both 0°, the Rician CDF agrees well with the Monte Carlo result.

VI. STATISTICAL ANALYSIS OF THE ARRAY RP

So far, we verified that the Beckmann distribution agrees with the Monte Carlo result and that the Rician distribution also fits the Monte Carlo result with deviation at certain

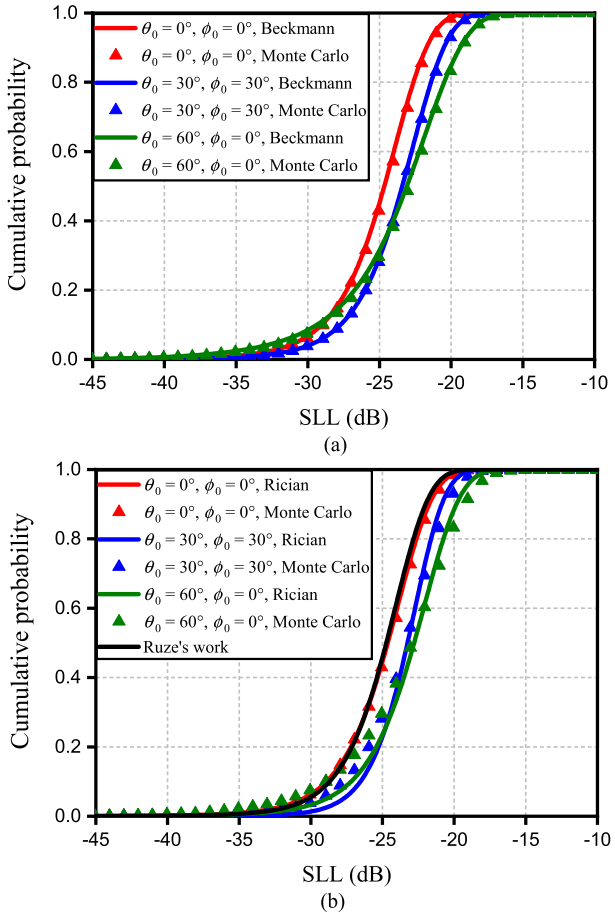

Fig. 4. SLL cumulative distribution of 8×8 planar antenna array. Each distribution was calculated at the position where h is maximum. (a) Beckmann distribution versus Monte Carlo simulation result for three steering angles. (b) Rician distribution versus Monte Carlo simulation result for three steering angles, along with Ruze's work for comparison [6].

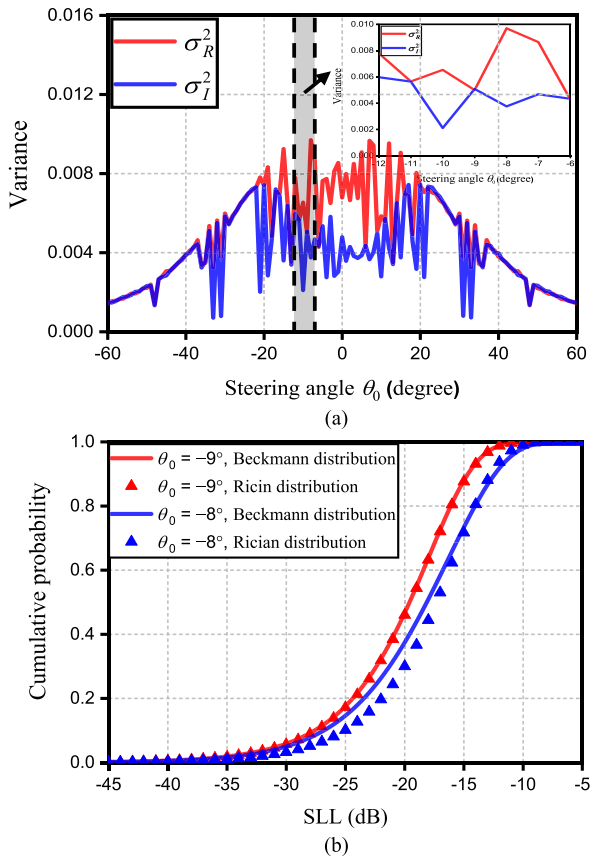

Fig. 5. (a) Variances of real and imaginary RP as steering angle changes. (b) Rician versus Beckmann distributions when steering angles θ_0 are $-9°$ and $-8°$.

steering angles. In this section, the effect of the steering angle on SLL probability is explained. Next, the maximum probability of exceeding a certain RP level is presented for specific steering angles. For simplicity and clarity, an eight-element uniform linear array located on the y-axis with antenna spacing of half-lambda is assumed and only θ is used to represent the RP of the array ($\phi = \pi/2$). The parameters in Table I were used again for simulation. To extract mutual coupling parameters, a 1×8 linear dipole array with relatively large coupling between antennas was designed on a Rogers RT/duroid 5880 substrate with 0.508 mm thickness. Total dipole length was 0.39 cm, and spacing between adjacent antennas was a half-wavelength of 28.5 GHz.

A. Steering Effect

The variances of the RP depend on the steering angle. Fig. 5 shows how the variances for real and imaginary RP components vary with respect to the steering angle from (28) and (29), along with the CDFs from the two solutions based on the Beckmann and Rician functions at two steering angles with small separation. At $\theta_0 = -9°$, the Beckmann distribution and Rician distribution show fairly good agreement with each other.

However, when we shift the steering direction to $\theta_0 = -8°$, the difference in the SLL between the two solutions becomes around 1 dB or more for the CDF ranging from 0.1 to 0.5. The difference arises from the approximation we made for the Rician-based solution: the real and imaginary components of the RP are independent, and the variance is identical to the average value of their variances. As can be seen in Fig. 5(a), the two variances fluctuate a lot depending on the steering angle, and the assumption for the Rician function is not valid in a wide range of steering angles. In addition, according to antenna array theory, this behavior depends on random errors, antenna separation, the number of antennas, and so on. Thus, even though the approximate solution modeled in the Rician distribution function shows better accuracy than prior work due to its reflecting the three major errors, it inherently cannot estimate all operation conditions for a given antenna array accurately.

B. Worst CDF of SLL

$p_{\max}(x_0)$ is usually estimated at the angle with the highest sidelobe of the RP mean h. When only random error is considered, σ_{aver}^2 is derived as a constant with respect to elevation angle θ. Therefore, it is obvious that the highest

sidelobe will limit $p_{\max}(x_0)$ [6], [7], [27]. However, this is not always valid when the effects of the quantization error and mutual coupling are added into this analysis. The parameters in Table I were used again at, for instance, an 18° steering angle, and the results are shown in Fig. 6. Fig. 6(a) and (b) shows the mean of RPs and CDFs of the SLL at the four highest sidelobes with the exact solution in the Beckmann distribution, where θ_{SL1}, θ_{SL2}, θ_{SL3}, and θ_{SL4} represent the first, second, third, and fourth peak sidelobe of the RP mean, respectively. As can be seen in Fig. 6(b), in the region of the SLL > -18 dB, the CDF at the second sidelobe (SL2) at θ_{SL2} is slightly worse than the CDF at the first sidelobe (SL1) at θ_{SL1}. Fig. 6(c) shows $p_{\max}(x_0 = -12\ \mathrm{dB})$ as a function of θ. The main lobe area in the gray zone is not considered in this analysis. As can be seen, $p_{\max}$ values at θ_{SL1} and θ_{SL2} are approximately 1.3% and 3.9%, respectively. According to the RP mean, SL2 is estimated to influence the system performance slightly less than SL1, but the interfering signal would indeed be coupled at θ_{SL2} through SL2 with three times larger probability than through SL1. Even worse, $p_{\max}$ caused by the fourth peak (SL4) at θ_{SL4}, whose mean is around 4 dB smaller than that of SL1, is approximately 2.5%, two times higher than that caused by SL1. These results can be explained by the variance with respect to the elevation angle depicted in Fig. 6(d). As can be seen, the variance of SL4 is approximately 1.5 times larger than that of SL1, implying the magnitude of SL4 fluctuates in a large range and exceeds a certain level more frequently than SL1 does. Thus, in analyzing the statistical interference due to the sidelobes, variance should be taken into account together with the mean value.

Here, let us look at the SL2 results in Fig. 6(c) and (d) again. The variances of real and imaginary RP components are not equal; therefore, as can be seen in Fig. 6(c), the Rician-based solution assuming σ_R^2 and σ_I^2 are equal underestimates the impact of SL2 by 30% or more in this example. The approximate solution offers reasonable agreement overall, but at the specific elevation angle where σ_R^2 and σ_I^2 have large disparity, one may fail to accurately estimate the system performance.

In Fig. 7, the distribution of the real and imaginary RP components is graphically visualized from the Monte Carlo simulation using the parameters in Table I and (16) for the cases of SL1 and SL2 in Fig. 6. The radius from the origin represents the SLL, and the mean value of the RP at the given elevation angle is the radius from the origin to the blue dot. Fig. 8 shows the correlation between R_{RP} and I_{RP} from (33). For SL1, σ_R^2 and σ_I^2 are nearly equal, and R_{RP} and I_{RP} are not correlated. Thus, the contour profile shown in Fig. 7(a) occupies the circular area, and the area far from the origin rarely exceeds the -12 dB bound. On the other hand, the RP for SL2 shows an elliptical profile that is slightly tilted 25° from the x-axis. Since σ_R^2 is larger than σ_I^2, the RP largely fluctuates along the real axis with the finite correlation shown in Fig. 8 and often exceeds the reference level of -12 dB. In Fig. 7(c) and (d), the effect of the variance is visualized. In the case of SL3 and SL4, though the mean values of both RPs are comparable, as shown in Fig. 6(a), the variance

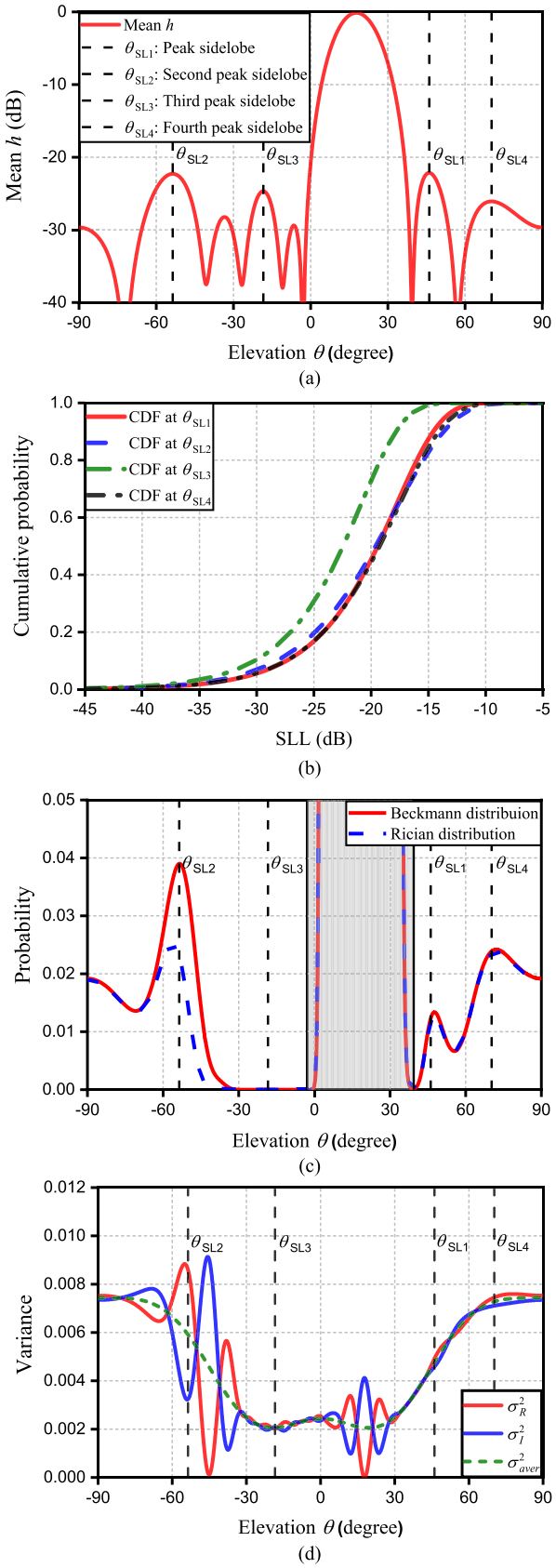

Fig. 6. (a) Mean value h of eight-element linear antenna array. (b) Beckmann distribution calculated at the elevation angles (θ_{SL1}, θ_{SL2}, θ_{SL3}, and θ_{SL4}). (c) Probability $p_{\max}(x_0 = -12\mathrm{dB})$ of SLL that is higher than -12 dB. (d) Variance of R_{RP} and I_{RP} and their average variance.

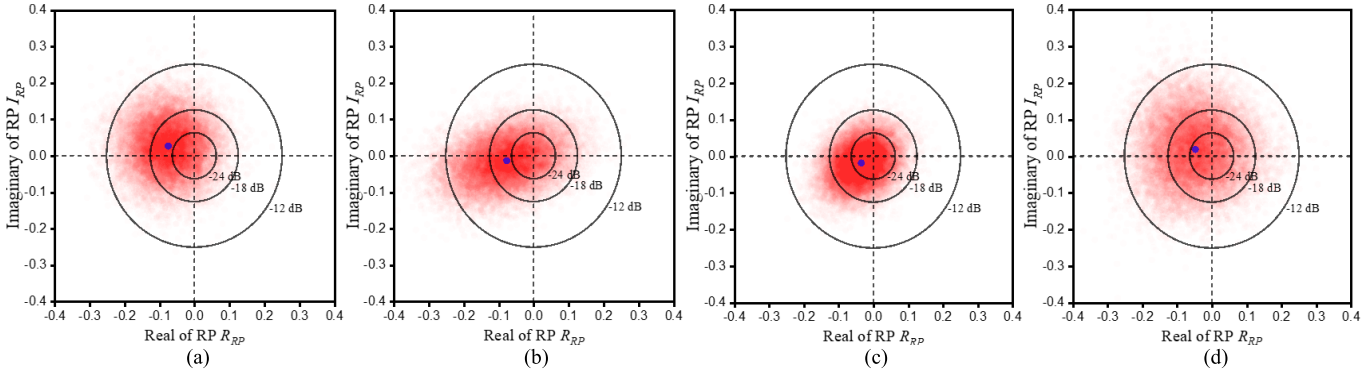

Fig. 7. Scatter plots of R_{RP} and I_{RP} at (a) θ_{SL1}, (b) θ_{SL2}, (c) θ_{SL3}, and (d) θ_{SL4}.

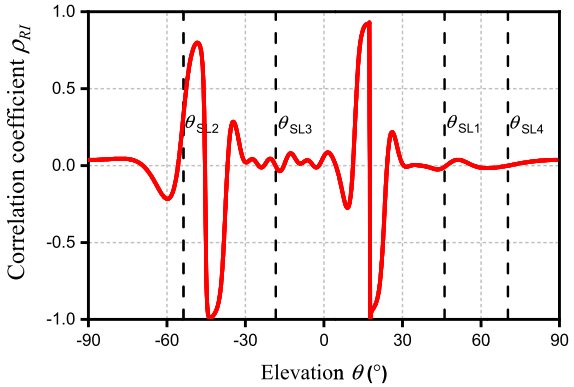

Fig. 8. Correlation coefficient between real and imaginary RP.

of SL3 is approximately one fourth of the variance of SL4. As illustrated in Fig. 7(c) and (d), the complex RP for SL4 is widely spread in the space, while the RP for SL3 is relatively concentrated in the space below −18 dB with high probability, which is consistent with the CDF shown in Fig. 6(b). These diagrams clearly show that the mean of the RP will not provide a precise interference analysis of an analog beamforming system. These results most likely arise from the quantization error and mutual coupling that make the statistical behaviors of the RPs strongly depend on the main beam direction and elevation angle.

VII. Conclusion

In this article, we investigated distorted RPs and derived their statistical behavior due to random error, quantization error, and mutual coupling. From the RPs distorted by the three errors, statistical parameters were derived. Then, we showed that the Beckmann distribution provides an exact solution representing the statistical behavior of RPs with high accuracy. Even under the assumption of the Rician distribution, the approximate solution provided good agreement with Monte Carlo simulation results and represented important characteristics of the distorted RPs overall, which could not be analyzed in prior studies. Since the variance of the RP fluctuates a lot with respect to the beam steering direction, azimuth angle, and elevation angle, a simple analysis with the mean value is not good enough for evaluating the interference performance of an analog beamforming antenna. In particular, the average variance with mutual coupling at certain θ and ϕ can be higher than the average variance with no mutual coupling. In this case, the maximum probability of exceeding a certain SLL may not be obtained at the angle of the highest sidelobe in the mean of the RPs. The maximum probability may be found from the Beckmann distributions calculated at all side lobes as the steering angle changes within the scanning range of the array antenna system. Ultimately, the accurate PDF of the RP considering all the errors and mutual coupling in this work will serve as an important basis of techniques for accurate phased array antenna calibration.

Appendix

A. Variance and Correlation Derivation

RP distorted by the three errors is expressed as

$$F_d(\phi) = \sum_{m=1}^{M}\sum_{n=1}^{N}\left(\sum_{p=1}^{M}\sum_{q=1}^{N} A_{pq} C_{mn,pq}(1+\delta_{pq}^{\mathrm{A}}) \times (1+\Delta_{pq}^{\mathrm{A}}) e^{j\left(\delta_{pq}^{\mathrm{P}}+\Delta_{pq}^{\mathrm{P}}\right)}\right) e^{j(mu+nv)}. \quad \text{(A.1)}$$

From (16), (19), and (20), the distorted RP can be separated into real and imaginary terms as

$$F_d = R_{RP} + jI_{RP}. \quad \text{(A.2)}$$

The variance and covariance of the real and imaginary RP can be calculated from variance (A.3) and pseudo-variance (A.6)

$$\mathrm{E}[|F_d - \mathrm{E}[F_d]|^2] = \sigma_R^2 + \sigma_I^2 \quad \text{(A.3)}$$

where

$$\mathrm{E}[(R_{RP} - \mathrm{E}[R_{RP}])^2] = \sigma_R^2 \quad \text{(A.4)}$$
$$\mathrm{E}[(I_{RP} - \mathrm{E}[I_{RP}])^2] = \sigma_I^2 \quad \text{(A.5)}$$
$$\mathrm{E}[(F_d - \mathrm{E}[F_d])^2] = \sigma_R^2 - \sigma_I^2 + 2j\sigma_{RI} \quad \text{(A.6)}$$

where

$$\sigma_{RI} = \mathrm{E}[(R_{RP} - \mathrm{E}[R_{RP}])(I_{RP} - \mathrm{E}[I_{RP}])]. \quad \text{(A.7)}$$

To summarize the above equations, the variance of each real and imaginary RP and covariance can be represented by using (A.3) and (A.6)

$$\sigma_R^2 = \frac{(\mathrm{E}[|F_d - \mathrm{E}[F_d]|^2] + \mathrm{Re}(\mathrm{E}[(F_d - \mathrm{E}[F_d])^2]))}{2} \quad \text{(A.8)}$$

$$\sigma_I^2 = \frac{(\mathrm{E}[|F_d - \mathrm{E}[F_d]|^2] - \mathrm{Re}(\mathrm{E}[(F_d - \mathrm{E}[F_d])^2]))}{2} \quad \text{(A.9)}$$

$$\sigma_{RI} = \frac{\mathrm{Im}(\mathrm{E}[(F_d - \mathrm{E}[F_d])^2])}{2}. \quad \text{(A.10)}$$

We can find the three parameters by deriving the variance and pseudo-variance of F_d.

To derive the variance of F_d, the expected value of $|F_d|^2$ can be represented as

$$\begin{aligned}
&\mathrm{E}\left[|F_d|^2\right] \\
&\quad = \mathrm{E}\left[F_d F_d^*\right] \\
&\quad = \mathrm{E}\Bigg[\Bigg(\sum_{m=1}^{M}\sum_{n=1}^{N}\Bigg(\sum_{p=1}^{M}\sum_{q=1}^{N} A_{pq}C_{mn,pq} \\
&\qquad \cdot\left(1+\delta_{pq}^{\mathrm{A}}\right)\left(1+\Delta_{pq}^{\mathrm{A}}\right)e^{j\left(\delta_{pq}^{\mathrm{P}}+\Delta_{pq}^{\mathrm{P}}\right)}\Bigg)e^{j(mu+nv)}\Bigg) \\
&\qquad \cdot\Bigg(\sum_{a=1}^{M}\sum_{b=1}^{N}\Bigg(\sum_{c=1}^{M}\sum_{d=1}^{N} A_{cd}C_{ab,cd} \\
&\qquad \cdot\left(1+\delta_{cd}^{\mathrm{A}}\right)\left(1+\Delta_{cd}^{\mathrm{A}}\right)e^{j\left(\delta_{cd}^{\mathrm{P}}+\Delta_{cd}^{\mathrm{P}}\right)}\Bigg)e^{j(au+bv)}\Bigg)^*\Bigg].
\end{aligned} \quad \text{(A.11)}$$

Because quantization error is static error for a given array amplitude weight and fixed steering angle, we use V_{pq}^{Q} instead of $A_{pq}(1+\Delta_{pq}^{\mathrm{A}})e^{j\Delta_{pq}^{\mathrm{P}}}$. Equation (A.11) can be expressed separately for $p=c$ and $q=d$, $p\neq c$ *or* $q\neq d$ as

$$\mathrm{E}\left[F_d F_d^*\right] = \mathrm{A} + \mathrm{B} \quad \text{(A.12)}$$

$$\begin{aligned}
\mathrm{A} = &\sum_{m=1}^{M}\sum_{n=1}^{N}\sum_{a=1}^{M}\sum_{b=1}^{N}\Bigg(\sum_{p=1}^{M}\sum_{q=1}^{N} V_{pq}^{Q}C_{mn,pq}\left(V_{pq}^{Q}C_{ab,pq}\right)^* \\
&\cdot\mathrm{E}\left[1+2\delta_{pq}^{\mathrm{A}}+\left(\delta_{pq}^{\mathrm{A}}\right)^2\right]e^{j[(m-a)u+(n-b)v]}\Bigg)
\end{aligned} \quad \text{(A.13)}$$

$$\begin{aligned}
\mathrm{B} = &\sum_{m=1}^{M}\sum_{n=1}^{N}\sum_{a=1}^{M}\sum_{b=1}^{N} \\
&\Bigg(\sum_{p=1}^{M}\sum_{q=1}^{N}\sum_{c=1,p\neq c}^{M}\sum_{d=1,q\neq d}^{N} V_{pq}^{Q}C_{mn,pq}\left(V_{cd}^{Q}C_{ab,cd}\right)^* \\
&\cdot\mathrm{E}\left[1+\delta_{pq}^{\mathrm{A}}+\delta_{cd}^{\mathrm{A}}+\delta_{pq}^{\mathrm{A}}\delta_{cd}^{\mathrm{A}}\right]\cdot\mathrm{E}\left[e^{j\left(\delta_{pq}^{\mathrm{P}}-\delta_{cd}^{\mathrm{P}}\right)}\right]e^{j[(m-a)u+(n-b)v]}\Bigg).
\end{aligned} \quad \text{(A.14)}$$

Because $\delta_{pq}^{\mathrm{A}}, \delta_{cd}^{\mathrm{A}}, \delta_{pq}^{\mathrm{P}}, \delta_{cd}^{\mathrm{P}}$ are assumed to be independent Gaussian random variables by (17) and (18), expected values in (A.13) and (A.14) can be derived as

$$\begin{aligned}
&\mathrm{E}\left[1+2\delta_{pq}^{\mathrm{A}}+\left(\delta_{pq}^{\mathrm{A}}\right)^2\right] \\
&\quad = \mathrm{E}[1] + 2\cdot\mathrm{E}\left[\delta_{pq}^{\mathrm{A}}\right] + \mathrm{E}\left[\left(\delta_{pq}^{\mathrm{A}}\right)^2\right] \\
&\quad = 1 + 0 + \sigma_a^2 = 1 + \sigma_a^2
\end{aligned} \quad \text{(A.15)}$$

$$\begin{aligned}
&\mathrm{E}\left[1+\delta_{pq}^{\mathrm{A}}+\delta_{cd}^{\mathrm{A}}+\delta_{pq}^{\mathrm{A}}\delta_{cd}^{\mathrm{A}}\right] \\
&\quad = \mathrm{E}[1] + \mathrm{E}\left[\delta_{pq}^{\mathrm{A}}\right] + \mathrm{E}\left[\delta_{cd}^{\mathrm{A}}\right] + \mathrm{E}\left[\delta_{pq}^{\mathrm{A}}\delta_{cd}^{\mathrm{A}}\right] \\
&\quad = 1 + 0 + 0 + 0 = 1
\end{aligned} \quad \text{(A.16)}$$

$$\begin{aligned}
\mathrm{E}\left[e^{j\left(\delta_{pq}^{\mathrm{P}}-\delta_{cd}^{\mathrm{P}}\right)}\right] &= \int_{-\infty}^{\infty}\int_{-\infty}^{\infty} e^{j\left(\delta_{pq}^{\mathrm{P}}-\delta_{cd}^{\mathrm{P}}\right)}d\delta_{pq}^{\mathrm{P}}d\delta_{cd}^{\mathrm{P}} \\
&= \int_{-\infty}^{\infty} e^{j\delta_{pq}^{\mathrm{P}}}d\delta_{pq}^{\mathrm{P}}\cdot\int_{-\infty}^{\infty} e^{-j\delta_{cd}^{\mathrm{P}}}d\delta_{cd}^{\mathrm{P}} \\
&= \mathrm{E}\left[e^{j\delta_{pq}^{\mathrm{P}}}\right]\mathrm{E}\left[e^{-j\delta_{cd}^{\mathrm{P}}}\right].
\end{aligned} \quad \text{(A.17)}$$

By using the Maclaurin series of the exponential function [28], the expected value of $e^{j\delta_{pq}^{\mathrm{P}}}, e^{-j\delta_{cd}^{\mathrm{P}}}$ in (A.17) can be derived as

$$e^x = 1 + x + \frac{x^2}{2} + \frac{x^3}{6} + \frac{x^4}{24} + \cdots \quad \text{(A.18)}$$

$$\begin{aligned}
\mathrm{E}\left[e^{j\delta_{pq}^{\mathrm{P}}}\right] &= \int_{-\infty}^{\infty} e^{j\delta_{pq}^{\mathrm{P}}}d\delta_{pq}^{\mathrm{P}} \\
&= \int_{-\infty}^{\infty}\Bigg(1 + j\delta_{pq}^{\mathrm{P}} - \frac{\left(\delta_{pq}^{\mathrm{P}}\right)^2}{2} \\
&\qquad - j\frac{\left(\delta_{pq}^{\mathrm{P}}\right)^3}{6} + \frac{\left(\delta_{pq}^{\mathrm{P}}\right)^4}{24} + \ldots\Bigg)d\delta_{pq}^{\mathrm{P}} \\
&= 1 - \frac{\sigma_p^2}{2} + \frac{\sigma_p^4}{8} + \cdots \\
&= 1 + \left(-\frac{\sigma_p^2}{2}\right) + \frac{1}{2}\left(-\frac{\sigma_p^2}{2}\right)^2 + \cdots \\
&= e^{-\sigma_p^2/2}
\end{aligned} \quad \text{(A.19)}$$

$$\mathrm{E}\left[e^{-j\delta_{cd}^{\mathrm{P}}}\right] = \mathrm{E}\left[e^{j\delta_{cd}^{\mathrm{P}}}\right]^* = e^{-\sigma_p^2/2}. \quad \text{(A.20)}$$

If we substitute (A.15)–(A-17), (A.19), and (A.20) into (A.13) and (A.14), (A.12) can be represented as

$$\begin{aligned}
&\mathrm{E}\left[F_d F_d^*\right] \\
&= \left(1+\sigma_a^2\right)\cdot\sum_{m=1}^{M}\sum_{n=1}^{N}\sum_{a=1}^{M}\sum_{b=1}^{N}\sum_{p=1}^{M}\sum_{q=1}^{N} V_{pq}^{Q}C_{mn,pq}\left(V_{pq}^{Q}C_{ab,pq}\right)^* \\
&\quad\cdot e^{j[(m-a)u+(n-b)v]} \\
&\quad + e^{-\sigma_p^2}\cdot\sum_{m=1}^{M}\sum_{n=1}^{N}\sum_{a=1}^{M}\sum_{b=1}^{N}\sum_{p=1}^{M}\sum_{q=1}^{N} \\
&\quad\sum_{c=1,p\neq c}^{M}\sum_{d=1,q\neq d}^{N} V_{pq}^{Q}C_{mn,pq}\left(V_{cd}^{Q}C_{ab,cd}\right)^* \\
&\quad\cdot e^{j[(m-a)u+(n-b)v]}.
\end{aligned} \quad \text{(A.21)}$$

By eliminating the condition $p\neq c$ *or* $q\neq d$ in the second summation term of (A.21), (A.21) can be expressed as

$$\begin{aligned}
\mathrm{E}\left[F_d F_d^*\right] = &\left(1+\sigma_a^2-e^{-\sigma_p^2}\right)\cdot\sum_{m=1}^{M}\sum_{n=1}^{N}\sum_{a=1}^{M} \\
&\sum_{b=1}^{N}\sum_{p=1}^{M}\sum_{q=1}^{N} V_{pq}^{Q}C_{mn,pq}\left(V_{pq}^{Q}C_{ab,pq}\right)^* \\
&\cdot e^{j[(m-a)u+(n-b)v]} \\
&+ e^{-\sigma_p^2}\cdot\sum_{m=1}^{M}\sum_{n=1}^{N}\sum_{a=1}^{M}\sum_{b=1}^{N}
\end{aligned}$$

$$\sum_{p=1}^{M}\sum_{q=1}^{N}\sum_{c=1}^{M}\sum_{d=1}^{N} V_{pq}^{Q} C_{mn,pq}\left(V_{cd}^{Q} C_{ab,cd}\right)^{*} \cdot e^{j[(m-a)u+(n-b)v]}. \tag{A.22}$$

By using (A.1) and (A.19), the expected values of F_d, F_d^*can be expressed as

$$\mathrm{E}[F_d] = e^{-\sigma_p^2/2} \cdot \sum_{m=1}^{M}\sum_{n=1}^{N}\sum_{p=1}^{M}\sum_{q=1}^{N} V_{pq}^{Q} C_{mn,pq} e^{j[mu+nv]} \tag{A.23}$$

$$\mathrm{E}\left[F_d^*\right] = e^{-\sigma_p^2/2} \cdot \sum_{a=1}^{M}\sum_{b=1}^{N}\sum_{c=1}^{M}\sum_{d=1}^{N} \left(V_{cd}^{Q} C_{ab,cd}\right)^{*} e^{-j[au+bv]}. \tag{A.24}$$

By substituting (A.23) and (A.24) into (A.22), (A.22) can be expressed as

$$\begin{aligned}\mathrm{E}\left[F_d F_d^*\right] &= \left(1+\sigma_a^2 - e^{-\sigma_p^2}\right) \\ &\cdot \sum_{m=1}^{M}\sum_{n=1}^{N}\sum_{a=1}^{M}\sum_{b=1}^{N}\sum_{p=1}^{M}\sum_{q=1}^{N} V_{pq}^{Q} C_{mn,pq}\left(V_{pq}^{Q} C_{ab,pq}\right)^{*} \\ &\cdot e^{j[(m-a)u+(n-b)v]} + \mathrm{E}[F_d]\mathrm{E}\left[F_d^*\right].\end{aligned} \tag{A.25}$$

By using (A.3) and (A.25), $\sigma_R^2 + \sigma_I^2$ can be expressed as

$$\begin{aligned}\sigma_R^2 + \sigma_I^2 &= \left(1+\overset{2}{\underset{a}{\sigma}} - e^{-\sigma_p^2}\right) \\ &\cdot \sum_{m=1}^{M}\sum_{n=1}^{N}\sum_{a=1}^{M}\sum_{b=1}^{N}\sum_{p=1}^{M}\sum_{q=1}^{N} V_{pq}^{Q} C_{mn,pq}\left(V_{pq}^{Q} C_{ab,pq}\right)^{*} \\ &\cdot e^{j[(m-a)u+(n-b)v]}.\end{aligned} \tag{A.26}$$

To derive pseudo-variance of F_d, the expected value of F_d^2 is derived in this case

$$\begin{aligned}&\mathrm{E}\left[F_d^2\right] \\ &= \mathrm{E}\Bigg[\left(\sum_{m=1}^{M}\sum_{n=1}^{N}\left(\sum_{p=1}^{M}\sum_{q=1}^{N} A_{pq} C_{mn,pq} \cdot\left(1+\delta_{pq}^{\mathrm{A}}\right)\left(1+\Delta_{pq}^{\mathrm{A}}\right)e^{j\left(\delta_{pq}^{\mathrm{P}}+\Delta_{pq}^{\mathrm{P}}\right)}\right)e^{j(mu+nv)}\right) \\ &\cdot\left(\sum_{a=1}^{M}\sum_{b=1}^{N}\left(\sum_{c=1}^{M}\sum_{d=1}^{N} A_{cd} C_{ab,cd} \cdot\left(1+\delta_{cd}^{\mathrm{A}}\right)\left(1+\Delta_{cd}^{\mathrm{A}}\right)e^{j\left(\delta_{cd}^{\mathrm{P}}+\Delta_{cd}^{\mathrm{P}}\right)}\right)e^{j(au+bv)}\right)\Bigg].\end{aligned} \tag{A.27}$$

As derived before, (A.27) can also be expressed for $p = c$ and $q = d$, $p \neq c$ *or* $q \neq d$

$$\mathrm{E}\left[F_d^2\right] = \mathrm{A} + \mathrm{B} \tag{A.28}$$

$$\begin{aligned}\mathrm{A} &= \sum_{m=1}^{M}\sum_{n=1}^{N}\sum_{a=1}^{M}\sum_{b=1}^{N} \\ &\left(\sum_{p=1}^{M}\sum_{q=1}^{N} V_{pq}^{Q} C_{mn,pq}\left(V_{pq}^{Q} C_{ab,pq}\right)\right. \\ &\left.\cdot \mathrm{E}\left[1+2\delta_{pq}^{\mathrm{A}}+\left(\delta_{pq}^{\mathrm{A}}\right)^2\right]\mathrm{E}\left[e^{j2\delta_{pq}^{\mathrm{P}}}\right]e^{j[(m+a)u+(n+b)v]}\right)\end{aligned} \tag{A.29}$$

$$\begin{aligned}\mathrm{B} &= \sum_{m=1}^{M}\sum_{n=1}^{N}\sum_{a=1}^{M}\sum_{b=1}^{N} \\ &\left(\sum_{p=1}^{M}\sum_{q=1}^{N}\sum_{c=1,\,p\neq c}^{M}\sum_{d=1,q\neq d}^{N} V_{pq}^{Q} C_{mn,pq}\left(V_{cd}^{Q} C_{ab,cd}\right)\right. \\ &\cdot \mathrm{E}\left[1+\delta_{pq}^{\mathrm{A}}+\delta_{cd}^{\mathrm{A}}+\delta_{pq}^{\mathrm{A}}\delta_{cd}^{\mathrm{A}}\right] \\ &\left.\cdot \mathrm{E}\left[e^{j\left(\delta_{pq}^{\mathrm{P}}+\delta_{cd}^{\mathrm{P}}\right)}\right]e^{j[(m+a)u+(n+b)v]}\right).\end{aligned} \tag{A.30}$$

By using (A.19), expected values in (A.29) and (A.30) can be derived as

$$\begin{aligned}\mathrm{E}\left[e^{j\left(\delta_{pq}^{\mathrm{P}}+\delta_{cd}^{\mathrm{P}}\right)}\right] &= \int_{-\infty}^{\infty}\int_{-\infty}^{\infty} e^{j\left(\delta_{pq}^{\mathrm{P}}+\delta_{cd}^{\mathrm{P}}\right)} d\delta_{pq}^{\mathrm{P}} d\delta_{cd}^{\mathrm{P}} \\ &= \mathrm{E}\left[e^{j\delta_{pq}^{\mathrm{P}}}\right]\cdot\mathrm{E}\left[e^{j\delta_{cd}^{\mathrm{P}}}\right] = e^{-\sigma_p^2}\end{aligned} \tag{A.31}$$

$$\begin{aligned}\mathrm{E}\left[e^{j2\delta_{pq}^{\mathrm{P}}}\right] &= \int_{-\infty}^{\infty} e^{j2\delta_{pq}^{\mathrm{P}}} d\delta_{pq}^{\mathrm{P}} \\ &= \int_{-\infty}^{\infty}\left(1+j2\delta_{pq}^{\mathrm{P}} - \frac{\left(2\delta_{pq}^{\mathrm{P}}\right)^2}{2} - j\frac{\left(2\delta_{pq}^{\mathrm{P}}\right)^3}{6}\right. \\ &\qquad \left.+\frac{\left(2\delta_{pq}^{\mathrm{P}}\right)^4}{24}+\cdots\right)d\delta_r^{\mathrm{P}} \\ &= 1-2\sigma_p^2+2\sigma_p^4+\cdots \\ &= 1+\left(-2\sigma_p^2\right)+\frac{1}{2}\left(-2\sigma_p^2\right)^2+\cdots \\ &= e^{-2\sigma_p^2}.\end{aligned} \tag{A.32}$$

If we substitute (A.15), (A.16), (A.31), and (A.32) into (A.29) and (A.30), (A.28) can be represented as

$$\begin{aligned}\mathrm{E}\left[F_d^2\right] &= \left(1+\overset{2}{\underset{a}{\sigma}}\right)e^{-2\sigma_p^2}\cdot\sum_{m=1}^{M}\sum_{n=1}^{N}\sum_{a=1}^{M} \\ &\sum_{b=1}^{N}\sum_{p=1}^{M}\sum_{q=1}^{N} V_{pq}^{Q} C_{mn,pq}\left(V_{pq}^{Q} C_{ab,pq}\right) \\ &\cdot e^{j[(m+a)u+(n+b)v]} \\ &+ e^{-\sigma_p^2}\cdot\sum_{m=1}^{M}\sum_{n=1}^{N}\sum_{a=1}^{M}\sum_{b=1}^{N} \\ &\sum_{p=1}^{M}\sum_{q=1}^{N}\sum_{c=1,\,p\neq c}^{M}\sum_{d=1,q\neq d}^{N} V_{pq}^{Q} C_{mn,pq}\left(V_{cd}^{Q} C_{ab,cd}\right) \\ &\cdot e^{j[(m+a)u+(n+b)v]}.\end{aligned} \tag{A.33}$$

By eliminating the condition $p \neq c$ *or* $q \neq d$ in the second summation term of (A.33), (A.33) can be expressed as

$$\begin{aligned}\mathrm{E}\left[F_d^2\right] &= \left(\left(1+\overset{2}{\underset{a}{\sigma}}\right)e^{-2\sigma_p^2} - e^{-\sigma_p^2}\right) \\ &\cdot\sum_{m=1}^{M}\sum_{n=1}^{N}\sum_{a=1}^{M}\sum_{b=1}^{N}\sum_{p=1}^{M}\sum_{q=1}^{N} V_{pq}^{Q} C_{mn,pq}\left(V_{pq}^{Q} C_{ab,pq}\right) \\ &\cdot e^{j[(m-a)u+(n-b)v]} \\ &+ e^{-\sigma_p^2}\cdot\sum_{m=1}^{M}\sum_{n=1}^{N}\sum_{a=1}^{M}\end{aligned}$$

$$\sum_{b=1}^{N}\sum_{p=1}^{M}\sum_{q=1}^{N}\sum_{c=1}^{M}\sum_{d=1}^{N} V_{pq}^{Q} C_{mn,pq}\left(V_{cd}^{Q} C_{ab,cd}\right) \cdot e^{j[(m+a)u+(n+b)v]}. \tag{A.34}$$

By substituting (A.23) into (A.34), (A.34) can be expressed as

$$\begin{aligned}\mathrm{E}\left[F_d^2\right] = &\left(\left(1+\overset{2}{\underset{a}{\sigma}}\right)e^{-2\sigma_p^2} - e^{-\sigma_p^2}\right) \\ &\cdot \sum_{m=1}^{M}\sum_{n=1}^{N}\sum_{a=1}^{M}\sum_{b=1}^{N}\sum_{p=1}^{M}\sum_{q=1}^{N} V_{pq}^{Q} C_{mn,pq}\left(V_{pq}^{Q} C_{ab,pq}\right) \\ &\cdot e^{j[(m+a)u+(n+b)v]} \\ &+ \mathrm{E}[F_d]\mathrm{E}[F_d]. \end{aligned} \tag{A.35}$$

By using (A.6) and (A.35), $\sigma_R^2 - \sigma_I^2$ and σ_{RI} can be expressed as

$$\begin{aligned}\sigma_R^2 - \sigma_I^2 = &\left(\left(1+\overset{2}{\underset{a}{\sigma}}\right)e^{-2\sigma_p^2} - e^{-\sigma_p^2}\right) \\ &\cdot \sum_{m=1}^{M}\sum_{n=1}^{N}\sum_{a=1}^{M}\sum_{b=1}^{N}\sum_{p=1}^{M}\sum_{q=1}^{N} \\ &\cdot \mathrm{Re}\left(V_{pq}^{Q} C_{mn,pq} V_{pq}^{Q} C_{ab,pq} e^{j[(m+a)u+(n+b)v]}\right) \end{aligned} \tag{A.36}$$

$$\begin{aligned}2\sigma_{RI} = &\left(\left(1+\overset{2}{\underset{a}{\sigma}}\right)e^{-2\sigma_p^2} - e^{-\sigma_p^2}\right) \\ &\cdot \sum_{m=1}^{M}\sum_{n=1}^{N}\sum_{a=1}^{M}\sum_{b=1}^{N}\sum_{p=1}^{M}\sum_{q=1}^{N} \\ &\cdot \mathrm{Im}\left(V_{pq}^{Q} C_{mn,pq} V_{pq}^{Q} C_{ab,pq} e^{j[(m+a)u+(n+b)v]}\right). \end{aligned} \tag{A.37}$$

Finally, if we denote $A_{pq}(1+\Delta_{pq}^{\mathrm{A}})e^{j\Delta_{pq}^{\mathrm{P}}}$ instead of V_{pq}^{Q} reversely and use (A.8)–(A.10), (A.26), (A.36), and (A.37), σ_R^2, σ_I^2, and σ_{RI} can be summarized as

$$\sigma_R^2 = \mathrm{A} + \mathrm{B} \tag{A.38}$$

$$\sigma_I^2 = \mathrm{A} - \mathrm{B} \tag{A.39}$$

$$\sigma_{RI} = \mathrm{C} \tag{A.40}$$

where

$$\begin{aligned}\mathrm{A} = &\frac{1}{2}\left(1+\overset{2}{\underset{a}{\sigma}} - e^{-\sigma_p^2}\right) \\ &\cdot \sum_{m=1}^{M}\sum_{n=1}^{N}\sum_{a=1}^{M}\sum_{b=1}^{N}\sum_{p=1}^{M}\sum_{q=1}^{N} V_{pq}\left(1+\Delta_{pq}^{\mathrm{A}}\right) C_{mn,pq} \\ &\cdot \left(V_{pq}\left(1+\Delta_{pq}^{\mathrm{A}}\right) C_{ab,pq}\right)^{*} e^{j[(m-a)u+(n-b)v]} \end{aligned} \tag{A.41}$$

$$\begin{aligned}\mathrm{B} = &\frac{1}{2}\left(\left(1+\overset{2}{\underset{a}{\sigma}}\right)e^{-2\sigma_p^2} - e^{-\sigma_p^2}\right) \\ &\cdot \sum_{m=1}^{M}\sum_{n=1}^{N}\sum_{a=1}^{M}\sum_{b=1}^{N}\sum_{p=1}^{M}\sum_{q=1}^{N} \mathrm{Re}\left(V_{pq}\left(1+\Delta_{pq}^{\mathrm{A}}\right) C_{mn,pq}\right. \\ &\left.\cdot V_{pq}\left(1+\Delta_{pq}^{\mathrm{A}}\right) C_{ab,pq} e^{j[(m+a)u+(n+b)v]}\right) \end{aligned} \tag{A.42}$$

$$\begin{aligned}\mathrm{B} = &\frac{1}{2}\left(\left(1+\overset{2}{\underset{a}{\sigma}}\right)e^{-2\sigma_p^2} - e^{-\sigma_p^2}\right) \\ &\cdot \sum_{m=1}^{M}\sum_{n=1}^{N}\sum_{a=1}^{M}\sum_{b=1}^{N}\sum_{p=1}^{M}\sum_{q=1}^{N} \mathrm{Im}\left(V_{pq}\left(1+\Delta_{pq}^{\mathrm{A}}\right) C_{mn,pq}\right. \\ &\left.\cdot V_{pq}\left(1+\Delta_{pq}^{\mathrm{A}}\right) C_{ab,pq} e^{j[(m+a)u+(n+b)v]}\right). \end{aligned} \tag{A.43}$$

REFERENCES

[1] B. Sadhu *et al.*, "A 28-GHz 32-element TRX phased-array IC with concurrent dual-polarized operation and orthogonal phase and gain control for 5G communications," *IEEE J. Solid-State Circuits*, vol. 52, no. 12, pp. 3373–3391, Dec. 2017.

[2] R. Long, J. Ouyang, F. Yang, Y. Li, K. Zhang, and L. Zhou, "Calibration method of phased array based on near-field measurement system," in *Proc. IEEE Antennas Propag. Soc. Int. Symp. (APSURSI)*, Jul. 2014, pp. 1161–1162.

[3] H. Steyskal and J. S. Herd, "Mutual coupling compensation in small array antennas," *IEEE Trans. Antennas Propag.*, vol. 38, no. 12, pp. 1971–1975, Dec. 1990.

[4] T. Takahashi, Y. Konishi, S. Makino, H. Ohmine, and H. Nakaguro, "Fast measurement technique for phased array calibration," *IEEE Trans. Antennas Propag.*, vol. 56, no. 7, pp. 1888–1899, Jul. 2008.

[5] J. S. Herd and M. D. Conway, "The evolution to modern phased array architectures," *Proc. IEEE*, vol. 104, no. 3, pp. 519–529, Mar. 2016.

[6] J. Ruze, "The effect of aperture errors on the antenna radiation pattern," *Il Nuovo Cimento*, vol. 9, no. S3, pp. 364–380, Mar. 1952.

[7] K. J. Hsiao, "Array sidelobes, error tolerance, gain, and beamwidth," USA Nav. Res. Lab., Washington, DC, USA, Tech. Rep. 8841, Sep. 1984.

[8] C. J. Miller, "Minimizing the effects of phase quantization errors in an electronically scanned array," in *Proc. Symp. Electron. Scanned Phased Arrays Appl.*, vol. 1, Jul. 1964, pp. 17–38.

[9] A. J. van den Biggelaar, U. Johannsen, P. Mattheijssen, and A. B. Smolders, "Improved statistical model on the effect of random errors in the phase and amplitude of element excitations on the array radiation pattern," *IEEE Trans. Antennas Propag.*, vol. 66, no. 5, pp. 2309–2317, May 2018.

[10] R. Mailloux, *Phased Array Antenna Handbook*, vol. 2. Boston, MA, USA: Artech House, 2005.

[11] W. P. M. N. Keizer, "Low sidelobe phased array pattern synthesis with compensation for errors due to quantized tapering," *IEEE Trans. Antennas Propag.*, vol. 59, no. 12, pp. 4520–4524, Dec. 2011.

[12] W. Jiang, Y. Guo, T. Liu, W. Shen, and W. Cao, "Comparison of random phasing methods for reducing beam pointing errors in phased array," *IEEE Trans. Antennas Propag.*, vol. 51, no. 4, pp. 782–787, Apr. 2003.

[13] L. Lechtreck, "Cumulative coupling in antenna arrays," in *Proc. Antennas Propag. Soc. Int. Symp.*, vol. 3, Aug. 1965, pp. 144–149.

[14] W. Kahn, "Active reflection coefficient and element efficiency in arbitrary antenna arrays," *IEEE Trans. Antennas Propag.*, vol. AP-17, no. 5, pp. 653–654, Sep. 1969.

[15] S. Lee and H.-J. Song, "Investigation on statistical behavior of radiation pattern in analog beamforming system," in *Proc. IEEE Antennas Propag. Soc. Int. Symp. (APSURSI)*, Jul. 2020, pp. 595–596.

[16] N. Tyler, B. Allen, and H. Aghvami, "Adaptive antennas: The calibration problem," *IEEE Commun. Mag.*, vol. 42, no. 12, pp. 114–122, Dec. 2004.

[17] C. Galup-Montoro and M. C. Schneider, *MOSFET Modeling for Circuit Analysis and Design*. Singapore: World Scientific, 2007.

[18] K. R. Lakshmikumar, R. A. Hadaway, and M. A. Copeland, "Characterisation and modeling of mismatch in MOS transistors for precision analog design," *IEEE J. Solid-State Circuits*, vol. 21, no. 6, pp. 1057–1066, Dec. 1986.

[19] B. E. Stine, D. S. Boning, and J. E. Chung, "Analysis and decomposition of spatial variation in integrated circuit processes and devices," *IEEE Trans. Semicond. Manuf.*, vol. 10, no. 1, pp. 24–41, Feb. 1997.

[20] K. Kibaroglu, M. Sayginer, and G. M. Rebeiz, "An ultra low-cost 32-element 28 GHz phased-array transceiver with 41 dBm EIRP and 1.0–1.6 gbps 16-QAM link at 300 meters," in *Proc. IEEE Radio Freq. Integr. Circuits Symp. (RFIC)*, Honolulu, HI, USA, Jun. 2017, pp. 73–76.

[21] R. Mailloux, "Array grating lobes due to periodic phase, amplitude, and time delay quantization," *IEEE Trans. Antennas Propag.*, vol. AP-32, no. 12, pp. 1364–1368, Dec. 1984.

[22] R. Jedlicka, M. Poe, and K. Carver, "Measured mutual coupling between microstrip antennas," *IEEE Trans. Antennas Propag.*, vol. 29, no. 1, pp. 147–149, Jan. 1981.

[23] D. Segovia-Vargas, R. Martin-Cuerdo, and M. Sierra-Perez, "Mutual coupling effects correction in microstrip arrays for direction-of-arrival (DOA) estimation," *IEE Proc.-Microw., Antennas Propag.*, vol. 149, no. 2, pp. 113–118, Apr. 2002.

[24] J. W. Wallace and M. A. Jensen, "Mutual coupling in MIMO wireless systems: A rigorous network theory analysis," *IEEE Trans. Wireless Commun.*, vol. 3, no. 4, pp. 1317–1325, Jul. 2004.

[25] D. Parker and D. Z. Zimmermann, "Phased arrays—Part 1: Theory and architectures," *IEEE Trans. Microw. Theory Techn.*, vol. 50, no. 3, pp. 678–687, Mar. 2002.
[26] P. Beckmann, "Statistical distribution of the amplitude and phase of a multiply scattered field," *J. Res. Nat. Bureau Standards-D. Radio Propag.*, vol. 66, no. 3, pp. 231–240, 1962.
[27] C. M. Schmid, S. Schuster, R. Feger, and A. Stelzer, "On the effects of calibration errors and mutual coupling on the beam pattern of an antenna array," *IEEE Trans. Antennas Propag.*, vol. 61, no. 8, pp. 4063–4072, Aug. 2013.
[28] A. I. Markushevich, *Theory of Functions of a Complex Variable*, 2nd ed. New York, NY, USA: Chelsea, 1977.

Seunghoon Lee (Member, IEEE) received the B.S. degree in electrical engineering from the Pohang University of Science and Technology (POSTECH), Pohang, South Korea, in 2016, where he is currently pursuing the Ph.D. degree.

His research interests include phased-array antenna and millimeter-wave transmitter for wireless communication and radar.

Ho-Jin Song (Senior Member, IEEE) received the B. S. degree in electronics engineering from Kyungpook National University, Daegu, South Korea, in 1999, and the M.S. and Ph.D. degrees in electrical engineering from the Gwangju Institute of Science and Technology (GIST), Gwangju, South Korea, in 2001 and 2005, respectively.

He joined Nippon Telegraph and Telephone, Tokyo, Japan, in 2006, which is the third largest telecommunication company in the world, where he had engaged in the development of submillimeter and terahertz wave devices, circuits and systems for communication, remote sensing, and imaging applications. In 2015, he was named a Distinguished Research Scientist of NTT Labs, Kanagawa, Japan. Since 2016, he has been with the Department of Electrical Engineering, Pohang University of Science and Technology (POSTECH), Pohang, Gyeongbuk, South Korea, and is currently the Director of mm/THz Radio Research Center, established by the Ministry of Science and ICT, South Korea. His current research interests include mm-wave and terahertz circuits, antenna, packages and test-bed systems, particularly for wireless communication, connectivity, and radar applications.

Dr. Song was a recipient of GIST Best Thesis Award (2005), NTT Microsystem Labs Research of the Year Award (2009 and 2014), Young Scientist Award of Spectroscopical Society of Japan (2010), IEEE Microwave and Wireless Component Letters Tatsuo Itoh Best Paper Award (2014), and Best Industrial Paper Award at IEEE MTTs-IMS 2016 (2016). He is an IEEE distinguished microwave lecturer for the 2019–2021 term.